Synthesis of high surface area Cu/SiO_2 nanofiber catalysts for non-oxidative ethanol dehydrogenation

Tomas Pokorny[1#], Zdenek Kral[1#], Petr Machac[1], Zdenek Moravec[1], Lucie Simonikova[1], Vojtech Kundrat[2,3], Ales Styskalik[1*], Jiri Pinkas[1*]

[1]Department of Chemistry, Faculty of Science, Masaryk University, Kotlarska 2, CZ-61137 Brno, Czech Republic.
[2]Department of Molecular Chemistry and Materials Science, Weizmann Institute of Science, Rehovot 7610001, Israel.
[3]Thermo Fisher Scientific, CZ-62700 Brno, Czech Republic.

[*]Corresponding author's E-mail: styskalik@chemi.muni.cz (A. Styskalik), jpinkas@chemi.muni.cz (J. Pinkas).

[#] Tomas Pokorny and Zdenek Kral contributed equally to this work and should be considered co-first authors.

KEYWORDS. Heterogeneous catalyst; Ethanol dehydrogenation; Copper nanoparticles; Electrospinning; Polyvinylpyrrolidone; Nanofibers.

Abstract

Amidst growing concerns over the environmental impact of petroleum-based industries and their contribution to global ecological challenges, there is a pressing need for sustainable alternatives in chemical synthesis. This study addresses this imperative by exploring an innovative catalytic approach for the eco-friendly production of acetaldehyde from ethanol, a crucial chemical feedstock. Catalysts utilized so far perform poorly due to their low stability. Supported copper nanoparticles at higher temperatures suffer from the rapid deactivation caused by nanoparticles sintering and reduction of active sites by coking. To address this issue, the advanced copper nanoparticle-decorated silica nanofibres (107 nm in diameter) with outstanding surface area (700 $m^2 g^{-1}$) were synthesized and tested, showing enhanced stability in comparison to benchmark (Aerosil 300 SiO_2/Cu). Two approaches were compared for the preparation of copper catalyst, i.e., dry impregnation and one-pot synthesis. Remarkably, the dry-impregnated DI-9.4 sample at 325 °C after 100 h maintained over 66 % of ethanol conversion with 99 % selectivity to acetaldehyde (acetaldehyde productivity: 3.09 g g h^{-1}). This stability values surpass the benchmark catalyst, which dropped to 40 % of ethanol conversion. Our findings highlight the potential of the superior morphological advantage of electrospun SiO_2 nanofibers as an efficient catalyst.

1. Introduction

To develop a sustainable society, research should focus on the ecological issues and circular economy of chemical production.[1] Steam cracking remains an irreplaceable production mode for a large variety of chemicals, one of them being ethylene.[2] However, steam cracking is

an industrial process with the largest energy consumption and releasing the most significant amount of CO_2 (200 million tons of CO_2 emissions).[3] The Wacker process subsequently produces acetaldehyde from ethylene over homogeneous palladium catalysts.[4–6] New production pathways must be developed to substitute this non-sustainable and energy-demanding production based on crude oil.

Current trends in bioethanol research offer the possibility of using this resource for the production of more valuable chemicals including ethylene, acetaldehyde, and higher olefins.[7,8] Furthermore, the non-oxidative dehydrogenation of ethanol to acetaldehyde over a heterogeneous catalyst is a part of the butadiene production in the Lebedev or Ostromislenky process.[9] Thus, with tailored heterogeneous catalysts, bioethanol could replace a substantial part of petroleum-based chemistry.[10,11] Furthermore, its decreasing price positively affects the discussed and already ongoing transformation.[12]

Both experimental and theoretical works highlight copper's superiority as a catalyst for non-oxidative ethanol dehydrogenation: It is highly active and selective.[13] However, studies reveal two major challenges preventing its broad industrial application: the tendency of Cu nanoparticles (NPs) to produce coke and sinter during catalysis, both contributing to deactivation.[13–16]

The preparation method plays a crucial role in catalysis, as demonstrated in the Cu/SiO_2 (10 wt%) system. Ammonia evaporation (Cu NPs diameter 1.5–2.9 nm), deposition precipitation (23 nm), and wet impregnation (84 nm) techniques were used to deposit Cu on silica support. The Cu-phyllosilicate phases were observed in the case of ammonia evaporation procedure and surprisingly provided the most active and stable NPs.[15] One-pot methods usually lead to homogeneous Cu distribution within the catalyst and provide high activity.[17,18] Support composition also significantly influences catalytic performance. Ethanol dehydrogenation has been studied over Cu deposited on SiO_2[15,19] and carbon[13], which provided highly selective conversion to acetaldehyde (over 95 %), in contrast to ZrO_2 and ZnO catalyst supports.[20,21]

Besides the synthesis method and support composition, morphology could have a significant impact on the catalytic performance as well. However, this effect is only scarcely studied in detail. This is in striking contrast with the number of morphologies reported in the literature that arise from various synthetic procedures. Focusing on silica as a favorable catalyst support, the usual approach involves Cu impregnation on porous (commercial) SiO_2 matrices with different morphologies including fumed silica nanoparticles,[18] spray-dried silica microparticles with calibrated porosity,[17] (meso)porous silica gel,[22] etc.[23] Cu/SiO_2 catalysts with similar morphologies can also be prepared by one-pot synthesis methods.[17,18,24] Interestingly, all the above-mentioned studies focused on the differences brought by the synthesis methods (e.g., various impregnation methods, impregnation on support vs. one-pot synthesis) and neglected the influence of support and catalyst morphologies.

Nanofibers (NFs) represent an important materials morphology class studied with the main intention of increasing the surface-to-bulk atoms ratio, i.e., to increase the specific surface area. Importantly, high surface area can putatively lead to the improvement of catalytic performance. Nanofibers, similarly to other 1D structures (such as nanorods or nanowhiskers), attempt to increase the content of surface atoms by decreasing the diameter of the fibers.[25] In contrast to other 1D structures, nanofibers have the possibility to be formed into a variety of higher structures (e.g., nonwoven and woven materials), thus improving mechanical properties.[26] Furthermore, they enable better handling and bring more opportunities for commercial application. Interestingly, the application of NFs in heterogeneous catalysis has been reviewed recently, showing only a limited number of examples.[27]

Electrospinning is a synthetic technique for ultrathin fiber production. It is an electrohydrodynamic process in which a high voltage is applied to droplets to generate a thin jet of liquid that is accelerated toward a collector. During the flight of the jet, a solvent evaporates, and the liquid becomes a solid fiber that eventually reaches a collector.[28] Besides other factors, viscosity plays a critical role in the electrospinning process to maintain a continuous spinning process and to avoid defects, such as the formation of droplets or spraying.[29] Aside from the advantages in the synthesis and the morphology, the electrospinning technology has the potential to be scaled up to industrial scale production (e.g., industrial electrospinning from the free surface).[30] While organic polymers are widely prepared in the form of nanofibers via electrospinning[31], the synthesis of inorganic fibers remains more challenging due to post-spinning processes (calcination, reduction, sulfidation, and nitridation). Recently, silicotungstic acid was expediently utilized as a precursor for the pilot plant production of tungsten metal nanofibers[32] and WS_2 microfibers[33], both reinforced with amorphous silica. Various other challenging nanostructures, even from actinide oxides, were described previously (UO_2[34] and ThO_2[35]).

Patel et al. prepared SiO_2 nanofibers with an average diameter of 100 nm by using trimethoxysilyl-functionalized methacrylate copolymer as a precursor.[36] The most typical SiO_2 NFs preparation method studied in the literature includes the hydrolysis pre-gelation step in mixtures of TEOS, water, ethanol, and HCl.[37–42] This approach was studied by Choi et al. and synthesized fibers ranged between 200–600 nm in diameter.[42] The co-electrospinning of the pre-gelled sol-precursor and polymer (e.g., polyvinyl pyrrolidone, PVP) to improve the porosity of nanofibers was investigated. PVP not only controls the viscosity but also prevents crystallization and controls the surface area and pore size distribution in resulting nanofibers.[35,43] The advancing gelation of TEOS was addressed in the study of Geltmeyer et al.[44] where electrospinning was carried out after different times of TEOS hydrolysis and condensation at 60 °C. Results showed spinnability and structural changes related to viscosity that was affected by time, i.e., the viscosity increased with time. The changing viscosity has a negative impact on the morphology control, especially for slow-spun fibers with a low flow-through velocity, presenting an important drawback of this method. Finally, another commonly used approach for SiO_2 NFs preparation utilized already prepared silica nanoparticles for spinning. An average diameter of prepared nanofibres reached 150–1000 nm with less smooth and uniform surfaces.[45–47]

Herein, we present a novel non-gelling synthetic approach for SiO_2 and Cu/SiO_2 NFs one-pot preparation. We avoided the TEOS pre-gelation process and instead focused on the development of a stable electrospinning solution, which would be more suitable for long-time spinning (possibly industrial) without changing product properties. The presented method can reproducibly provide fibers with a relatively narrow diameter distribution. Furthermore, silica nanofibers prepared by electrospinning were applied as catalyst support. Particularly, these silica NFs were used to host Cu nanoparticles. The final Cu/SiO_2 nanofibrous catalysts prepared via one-pot synthesis and impregnation technique were tested for the first time in the non-oxidative dehydrogenation of ethanol to acetaldehyde. The highly promising catalytic performance, including stability with time-on-stream, is described. The decisive advantage of using nanofibrous catalysts is shown by a comparative experiment with a catalyst prepared by the same method with a nanoparticulate SiO_2 support.

2. Experimental Section

2.1. Materials

$Cu(NO_3)_2 \cdot 5/2H_2O$ (Merck) was used as a copper precursor in all reactions. Dimethylformamide (DMF) and tetraethyl orthosilicate (TEOS, 99 %) was purchased from Merck and used as received. Polyvinylpyrrolidone (PVP, 360 000 g mol^{-1}) and HCl (37 %) were purchased from Sigma Aldrich and were used without additional modification.

2.2. Synthesis

Preparation of electrospinning solutions

The solution for the synthesis of SiO_2 nanofibers (NFs) was prepared from PVP (1.2 g) dissolved in 9.0 g of DMF and stirred until a clear solution with no solid residues was formed. Then TEOS (2.5 g) was added dropwise to a rapidly stirred polymer solution. After a clear solution was formed, its conductivity was adjusted to 1.2 mS cm^{-1} by the dropwise addition of concentrated HCl (35 %) (**Table S1**). The protocol can be upscaled if needed.

For the one-pot (OP) synthesis of Cu/SiO_2 NFs, a similar protocol was pursued, with the exception that $Cu(NO_3)_2 \cdot 5/2H_2O$ (270 mg) was dissolved in the solution before the conductivity adjustment. The resulting solution was then vigorously stirred until the Cu precursor dissolved and a light blue solution was formed.

2.3. Electrospinning

A small lab-scale set-up was used for the electrospinning process. The prepared solution (approximately 20 cm^3) was loaded into a syringe with a metal needle (1.0 mm in diameter). To prevent solution dripping from the needle, a syringe pump was set to the flow rate of 3.5 µl min^{-1}. The distance from the needle tip to a collector was 15.0 cm and 15 kV of voltage was applied in total as +10 kV was applied to the needle and −5 kV to the collector. The drum collector (diameter 10 cm) covered with aluminium foil was rotating slowly at around 10 rpm. Prepared green NFs were calcined in a muffle furnace under static air using a heating rate of 10 °C min^{-1} to 500 °C. This temperature was maintained for additional 5 h. After this heat treatment, the material was left to cool down spontaneously.

2.4. Dry impregnation of SiO_2 NFs

A desired amount (Chyba! Nenalezen zdroj odkazů.) of $Cu(NO_3)_2 \cdot 5/2H_2O$ was dissolved in a minimal amount of water (6 g of H_2O per 1 g of NFs) to wet nanofibers completely. The solution and nanofibers were properly mixed, and the mixture was dried at 70 °C using a hotplate with magnetic stirring. The samples were calcined for 5 h at 500 °C in an ambient atmosphere after the drying process.

2.5. Reference sample

The reference sample (Cu/SiO_2) was prepared through dry impregnation on commercial silica Aerosil 300. $Cu(NO_3)_2{\cdot}5/2H_2O$ (458.1 mg, 1.970 mmol) was dissolved in a minimal volume of distilled water (50 cm^3) needed to fill the pores of the Aerosil 300 support and form a thick paste. The solution of the precursor was mixed with the silica support (5.00 g). The sample was placed in an oven (70 °C). After the drying process, the sample was ground into a fine powder and calcined (10 °C min^{-1}, 500 °C, 5 h).

2.6. Catalysis

A fix-bed catalytic reactor connected to a gas chromatograph was used for the catalytic reactions. The catalytic tests were performed at temperatures of 185, 220, 255, and 290 °C. One temperature step consisted of (i) a heating ramp (5 °C min^{-1}) and stabilization at the set temperature (21 min) and (ii) a steady temperature state (60 min at 185 and 220 °C; 84 min at 255 and 290 °C). The analysis of the effluent gas was carried out by an HP 6890 Gas Chromatograph (5 injections at 185 and 220 °C and 7 injections at 255 and 290 °C) equipped with a flame ionization detector (FID) and a Thermo Scientific TG-BOND U column (30 m long, internal diameter of 0.32 mm, film thickness of 10 µm). The stability experiments were carried out for 14 h at 325 °C.[18] Calcined catalysts (100 mg) were used for the catalytic reactions. All catalysts were adjusted to the same volume by glass beads (diam. 0.5−1 mm). The void space of the reactor was filled with glass beads. Before reactions, the catalysts were pre-treated in situ by forming gas (5 vol% H_2 in N_2, 52.5 cm^3 min^{-1} total flow) for 2 h at 325 °C to perform reduction of copper oxides. Pure nitrogen was used as a carrier gas (50 cm^3 min^{-1}) in all catalytic reactions; ethanol was fed by an NE-300 syringe pump with WHSV 4.73 h^{-1} (7.11 mol% of ethanol in N_2). Pentane (5 mol% in ethanol feed) was used as an internal standard. The tests were carried out at atmospheric pressure.

2.7. Characterization

Conductometry and viscosimetry measurements were used to characterize the prepared electrospinning solutions. The electrical conductivity of the solutions was measured with an XS Instrument Cond51 conductometer. An Alpha Fungilab rotational viscosimeter was used to measure viscosity. A PANalytical's EMPYREAN instrument was used for powder X-ray diffraction (PXRD). The samples were positioned on a spinning sample bed, and the Co lamp (λ = 1.78901 Å) was set to 20 mA and 30 kV. A semiconductor detector was used in a 1D mode. Catalyst coking was characterized using thermogravimetry (TG) with an STA 449 C Jupiter instrument by Netzsch. The samples were placed in platinum crucibles and subjected to heating in an airflow of 100 cm^3 min^{-1}, with a heating rate of 5 °C min^{-1}, reaching a maximum temperature of 1000 °C. Nominal elemental contents were determined by inductively coupled plasma optical emission spectroscopy (ICP-OES). ICP-OES analyses were done on an ICP-OES spectrometer iCAP PRO XPS Duo (Thermo, RF Power 1.10 kW, nebulizer gas flow 0.65 dm^3 min^{-}

[1], radial viewing height 11.0 mm). Emission lines 324.754 and 327.396 nm for Cu were used. X-ray photoelectron spectroscopy (XPS) was used as an alternate approach for coking assessment and elemental analysis. A Kratos Axis Supra instrument, outfitted with a monochromatic X-ray source and Al K_α (E = 1486.6 eV) excitation, was used to analyze the samples. As a calibration reference, binding energy of 284.8 eV for C1s was used. The specific surface area was determined through nitrogen porosimetry utilizing an Autosorb iQ3 instrument by Quantachrome Instruments. Measurements were conducted at a temperature of −195.7 °C to obtain adsorption and desorption isotherms. Prior to measurements, samples underwent degassing for a minimum of 12 h at 200 °C. The BET analysis provided specific surface area values from observed isotherms throughout a relative pressure range of 0.05 to 0.30. The micropore analysis was performed by the t-method. For the SEM analysis, a Versa 3D instrument manufactured by the Thermo Fischer Scientific company was used. Scanning was performed in a single or double lens mode using backscattered electrons or secondary electrons detection. All samples were plasma-coated with 5 nm of platinum. The diameter of fibers and distribution data were obtained using the ImageJ software by measurement of 50 unique fibers.[48] For the TEM analysis, the samples were dispersed by ultrasonication in isopropyl alcohol and drop-casted onto a copper grid with a lacey carbon film. EDS was measured on a Thermo Scientific Talos F200i equipped with a Bruker Dual-X spectrometer, operated in the STEM regime at a high voltage of 200 kV and beam current of 0.5 nA. Spectrum images were post-processed in the Velox software. Micrographs were analysed by the ImageJ program for the object's diameters.

3. Results and discussion

3.1. Synthesis of SiO_2 nanofibers

In this part of the study, SiO_2 NFs were synthesized reproducibly several times always yielding smooth surfaces and nearly uniform diameters. Electrospinning was carried out from a solution of TEOS and PVP in DMF with a very low amount of concentrated HCl necessary for increasing the solution conductivity and thus enabling the electrospinning process. This solution proved to be stable for months with no gelation observed. A pre-gelation step was not necessary, in contrast to other published water- or ethanol-based preparations of silica nanofibers that used the pregelation hydrolysis step (stirring at room temperature or at 80 °C in ethanolic solutions).[36,42–44] Geltmeyer et al. studied the effect of pre-gelation time and temperature on viscosity, which increased with the silane condensation.[44]

The preparation of SiO_2 NFs was completed by a calcination process (TGA record **Figure S1**) at 500 °C in air to remove PVP and finish the formation of SiO_2 NFs. It resulted in smooth nanofibers without defects with a relatively uniform thickness distribution, averaging about 107 nm in diameter (**Figure 1a** and **Table 1.**). The major benefits of using the virtually water- and

ethanol-free reaction system are the stability of the electrospinning solution and the consistency of product properties.

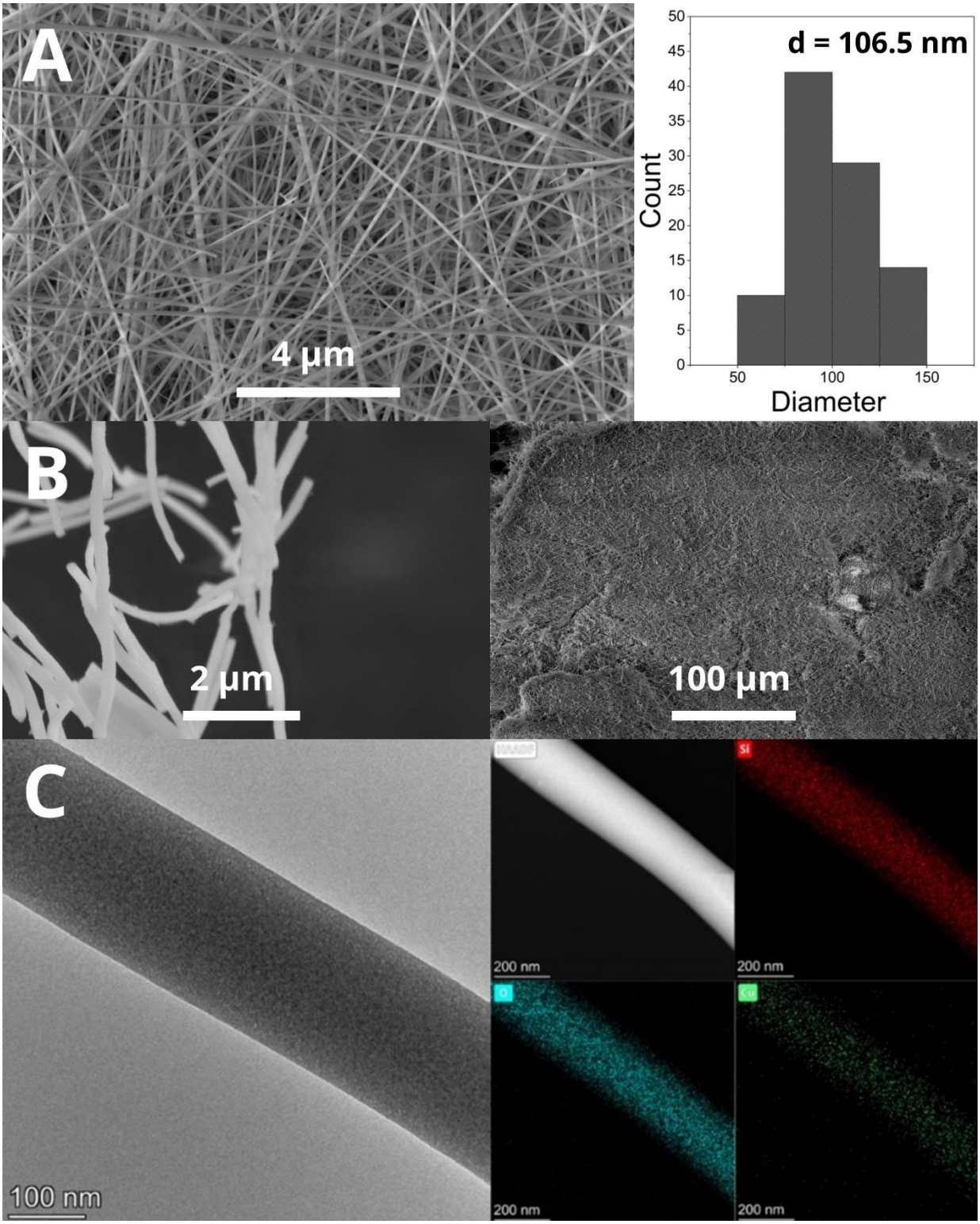

Figure 1. *Nanofibre catalysts characterization. A) SEM image of prepared SiO_2 nanofibers with histogram of diameter distribution, B) SEM image of DI-9.4 nanofibers (after Cu impregnation and calcination), C) Cu distribution in DI-9.4 nanofibers by STEM-EDS. Red represents silicon, blue oxygen, and green copper in EDS analysis.*

The preparation of Cu/SiO_2 NFs was performed by two methods. The one-pot (OP) approach utilized $Cu(NO_3)_2 \cdot 5/2H_2O$ as a Cu precursor, which was directly added to the electrospinning solution. The green NFs containing Cu in the whole volume were subsequently calcined in oxidizing atmosphere. The dry impregnation (DI) approach employed the silica NFs as a support. The SiO_2 NFs were impregnated with the aqueous solution of $Cu(NO_3)_2 \cdot 5/2H_2O$, dried and calcined in air.

3.2. Characterization of catalysts

The Cu/SiO_2 nanofiber samples prepared by two different methods (dry impregnation, DI, and one-pot synthesis, OP) were thoroughly characterized. Experimental values of actual Cu loadings analyzed by ICP-OES are shown in **Chyba! Nenalezen zdroj odkazů.**. The DI preparation method was straightforward with negligible deviations of copper concentration **(Table S2).** On the other hand, it was very difficult to maintain the desired Cu concentration for OP nanofibers. It was observed that the Cu concentration varies during the electrospinning process. At the beginning, Cu-rich nanofibers are produced, and as the spinning process advances, the Cu concentration decreases **(Table S3)**. This is probably due to a very slow flow rate through the needle (3–5 µl/min) and the applied voltage on the needle. Importantly, the Cu content in NFs stabilizes after the first 12 h from 104 h of the whole electrospinning time, and thus, it is possible to prepare Cu/SiO_2 NFs by the OP method with a well-defined Cu content.

The Cu content at the surface was determined by the XPS measurement (**Table 1**). In all samples the surface content was lower than the nominal and bulk (ICP-OES) copper loading. The XPS analysis of samples calcined in air revealed the presence of copper in oxidation state 1+ or 2+, which are hard to distinguish by the XPS technique (as discussed in detail below).

In **Table 1** and **S4**, the specific surface area (SSA) is compared for synthesized products as measured by N_2 porosimetry and corresponding N_2 isotherms are shown in **Figure S2**. In general, the DI samples are covered with an increasing amount of copper, which slightly decreases the surface area. The untreated SiO_2 NF material reached 700 $m^2\ g^{-1}$. The DI-1.8 and DI-5.1 had similar SSA of 609 and 604 $m^2\ g^{-1}$, respectively, while DI-9.4 exhibited somewhat lower SSA (542 $m^2\ g^{-1}$). The OP-6.5 sample featured the lowest SSA (473 $m^2\ g^{-1}$). For all the products, most of the surface area consisted of micropores (**Table S4**). The substantial microporosity of the NFs can be further evidenced by the isotherms (type I, **Figure S2**), relatively low pore volume (≤ 0.30 $cm^3\ g^{-1}$), and average pore diameter in the micropore range (0.89−1.1 nm; **Table S4**).

Table 1. Nanofiber samples and their properties.

Sample name	Average diameter [nm]	Standard deviation [nm]	Cu loading ICP-OES [wt%]	Surface Cu content XPS [wt%]	Surface area [$m^2\ g^{-1}$]	Pore volume [$cm^3\ g^{-1}$]
SiO2	107	24	-	-	700	0.35
DI-1.8	197	52	1.80	0.84	609	0.28
DI-5.1	168	26	5.11	0.54	604	0.29
DI-9.4	202	37	9.41	2.47	542	0.30
OP-6.5	365	43	6.46	1.36	473	0.21

The SEM analysis (Chyba! Nenalezen zdroj odkazů.**1b** and **Figure S3**) presents the morphology of prepared nanofiber catalysts. It showed smooth fibers. No significant defects in fiber morphology or crystallites of the copper oxide particles were observed. The average diameter of the DI NFs did not show any significant changes upon Cu content increase. The average fibre diameter for DI samples reached from 168 nm to 202 nm with a standard deviation from 26 to 52 nm. The OP sample with 6.5 wt% Cu (**OP-6.5**) gave rise to fibers with larger diameters, 365 nm on average, while the distribution remained relatively narrow (43 nm). The results of the graphic analysis are summarized in **Table 1.**

The aim of STEM and EDS analyses was to provide further insight into the fiber morphology and, especially the copper distribution in the fibers. A comparison of the EDS micrograph survey of samples prepared by **DI** and **OP** methods (**Figure 1c and S4**) points out that both methods resulted in evenly spread copper on the surface of the nanofibers. The STEM analyses displayed smooth texture, no apparent NP crystallization, and homogeneous copper distribution, i.e., without significant copper-rich centers. Only for the calcined DI-1.8 sample (Chyba! Nenalezen zdroj odkazů.Chyba! Nenalezen zdroj odkazů.**a**), the formation of small nanoparticles was found. The particles had a diameter of 3 nm (an average from a measurement of 30 unique particles), and it is very likely that the particles are made of copper oxide, although the STEM-EDS analysis did not show that explicitly. This is probably related to the imperfect dry impregnation preparation method.

None of the samples showed any significant diffractions before the catalytic activity tests, pointing to the XRD-amorphous character of the prepared NF catalysts (**Figure 2**). Apparently, copper-containing particles formed during calcination were too small and their content too low to be observed in PXRD. The formation of small nanoparticles, as was observed by STEM on the surface of the calcined sample DI-1.8 (Chyba! Nenalezen zdroj odkazů.**a**), has not been corroborated by the PXRD analyses, which reflect rather the bulk properties of the sample.

The PXRD analyses can be used for crystallite size estimation and comparison using the Debye-Scherrer equation. No significant diffractions were observed in the case of fresh nanofiber catalysts (**Figure 2**), and the application of the Debye-Scherrer equation was not possible. In our previous study,[18] fresh samples were prepared by dry impregnation method with 2.5 wt% of Cu using Aerosil-300 (mixture of SiO_2 aggregated nanoparticles) as catalyst

support. The estimated crystallite size by the Debye-Scherrer equation reached ~32 nm. In a study by Zhang et al.[22], Cu nanoparticles were prepared via the wet impregnation method with 10 wt% Cu loading supported on silica and exhibited ~84 nm crystallite size. The absence of diffractions points to a homogeneous Cu dispersion over SiO_2 NFs.

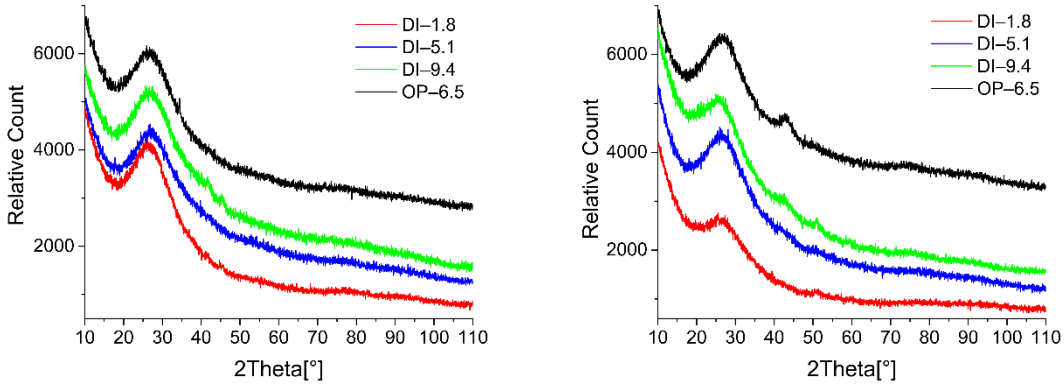

Figure 2. *PXRD diffractogram of NF catalysts. Left - fresh catalysts before the catalysis, right - spent catalysts after completed catalytic testing.*

The X-ray photoelectron spectroscopy was applied to study the copper oxidation state in the nanofibrous catalysts, (**Figure 3**). The satellite peak of Cu^{2+} species at ~943 eV[49] in all calcined nanofibers was present in the Cu 2p XPS spectra. A typical peak at ~935 eV[24] confirms the oxidized form of copper (**Table S5**). Therefore, a reduction pretreatment step was applied before catalysis to obtain metallic Cu in the nanofiber catalysts.[50] The XPS measurements of samples after catalytic reaction clearly displayed reduced Cu species and the presence of Cu^{1+} and Cu^0 only. These two states cannot be distinguished from each other (peak position at 933.2 eV, **Table S6**).[18,51] C 1s, O 1s, and Si 2s XPS spectra of all nanofiber catalysts are displayed in Supplemental materials (**Figure S5 and S6**). They feature typical C 1s XPS spectra of adventitious carbon,[52] and the O 1s and Si 2p spectra of oxygen and silicon in silica.[53–55] Both Si 2p and O 1s were slightly shifted by interaction with Cu as its loading increased. The detailed position of peaks, FWHM, ratios, and spin-orbital splittings are summarized in **Table S5** for fresh and in **Table S6** for spent catalysts.

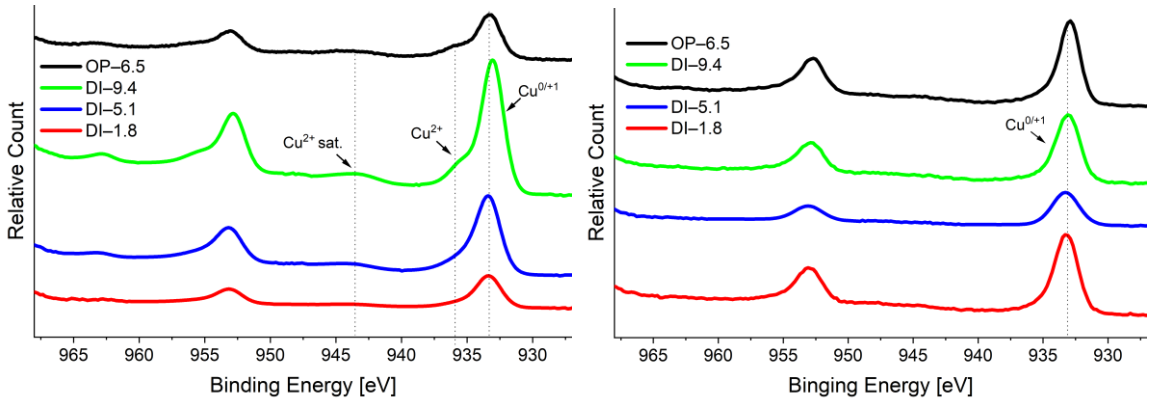

Figure 3. *XPS analyses, left - fresh catalysts before the catalysis, right - spent catalysts after completed catalytic testing.*

3.3. Catalytic activity tests

Catalysts prepared by the **DI** method showed different catalytic activity and stability with varying Cu concentrations (**Figure 4**)**.** Sample **DI-1.8** exhibited a decrease in catalytic activity mainly during the 290 °C run as it lost ~15 % of its activity (44 % to 29 % ethanol conversion drop in 84 min). On the contrary, no significant deactivation was observed for the samples **DI-5.1** and **DI-9.4**. The catalytic performance was in the case of these two samples similar. Ethanol conversion was at 185 °C around 20 %, and with the increasing temperature the conversion increased. At 220 °C, ethanol conversion kept stable around 45 %; at 255 °C, it was around 75 %; and at 290 °C, the ethanol conversion reached 90 % with no signs of deactivation. Acetaldehyde productivity reached 3.31 g g^{-1} h^{-1} for DI-9.4 at 255 °C outperforming most of the Cu/SiO_2 catalysts with similar Cu loading to date (**Table S7**).[18] The sample **OP-6.1** displayed a similar stability but it was less active than **DI-5.1** and **DI-9.4** in the runs at 255 °C (~65 % conversion) and 290 °C (~80 %).

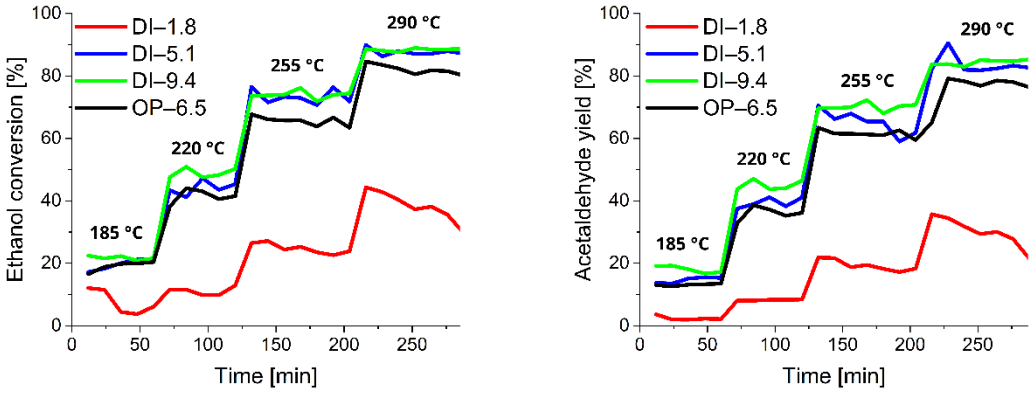

Figure 4. *Ethanol to acetaldehyde catalytic reaction over the NF catalysts with different Cu loading measured at 185, 220, 255, and 290 °C. Left - the ethanol conversion during the catalytic reaction, right - acetaldehyde yield.*

All prepared samples, apart from the **DI-1.8**, were highly selective to acetaldehyde. Selectivity at tested temperatures is plotted in **Figure 5.** The selectivity to acetaldehyde increased with ethanol conversion, only a small and constant amount of ethylene and diethyl ether was observed, and acetaldehyde was the major product during the whole reaction at all temperatures. The selectivity to acetaldehyde at 220–290 °C was in the range of 87–96 % and these values were even higher (95–97 %) at 325 °C for DI-5.1, DI-9.4, and OP-6.5. Low conversion and the deactivation of the **DI-1.8** caused a drop in acetaldehyde selectivity at high temperatures (52 %).

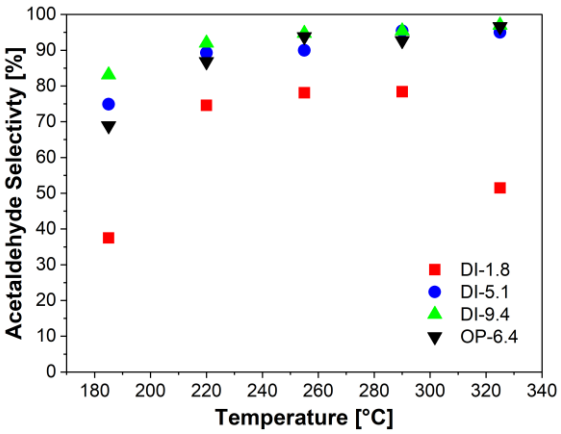

***Figure 5**. The selectivity to acetaldehyde in non-oxidative ethanol dehydrogenation over NF catalysts at different temperatures.*

The difference in the performance between **DI-5.1** and **DI-9.4** samples was pronounced mainly at 325 °C during long-term stability measurements (**Figure 6**). Both samples exhibited at the beginning ethanol conversion of 95 %. After 14 h, ethanol conversion dropped for the **DI-5.1** sample below 80 %, the sample **DI-9.4** remained stable and kept ethanol conversion above 90 % for the whole stability test. **DI-1.8** suffered from an extensive deactivation at 325 °C. The ethanol conversion at this temperature was only 30 % and dropped below 10 % after 19 h of catalytic testing. Despite the higher Cu loading of the **OP-6.5** sample, its stability and activity were worse than **DI-5.1** during the stability test.

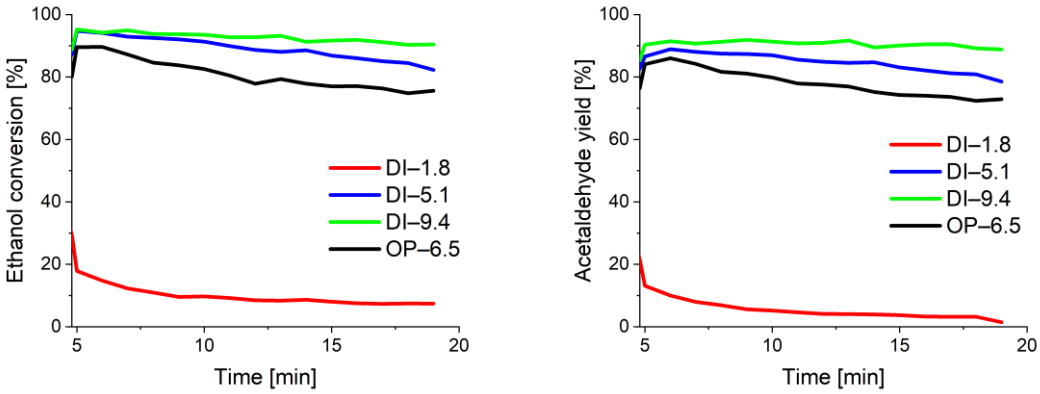

***Figure 6.** The stability measurement of NF catalysts at 325 °C. The chart compares samples of different Cu loading. Left - ethanol conversion, right - acetaldehyde yield.*

Extended deactivation testing of **DI-9.4** with time-on-stream (TOS) at 325 °C revealed a continuous decline in activity attributed to catalyst deactivation (**Figure 7**). After nearly 100 h of TOS at 325°C, the nanofiber catalyst **DI-9.4** experienced a ~25% reduction in ethanol conversion. Selectivity during TOS remained at ~98 % to acetaldehyde, and productivity to acetaldehyde after 100 h reached 3.09 g g^{-1} h^{-1}. A comparison with a 10 wt% Cu/SiO_2 catalyst prepared by dry impregnation on Aerosil 300 (considered the most stable preparation method according to our previous study[18]) demonstrated a significantly enhanced stability of the nanofibrous catalyst. Aerosil 300 with 7.2 wt% of Cu exhibited a rapid loss of ethanol conversion, losing around 25% within 15 h of TOS, and experiencing a decrease of over 45% in

ethanol conversion after 80 h. The final ethanol conversion after 80 h was 40 % with high average acetaldehyde selectivity (98 %). The productivity of acetaldehyde reached 1.85 g g h^{-1} (~60 % of **DI-9.4**). Oxidative regeneration (~20 % O_2 in N_2, 60 ml/min) at 500 °C proved that coking stands for the main reason for deactivation; the activity was completely restored. This observation is, on the one hand, in contrast to the observation by Petroliny et al.,[56] where initial conversion was not restored by O_2 regeneration: The deactivation on Cu/AlMgO was caused by particles sintering at 300 °C (10 wt% of Cu, WHSV = 4.7 h^{-1}). On the other hand, it agrees well with Pampararo et al., studying Cu deposited on silica microspheres prepared via aerosol-assisted sol-gel method.[17] Importantly, both catalysts (supported on Aerosil 300 and silica nanofibers) reached the initial activity after oxidative regeneration, and the sample supported on Aerosil 300 again deactivated more rapidly than the nanofibrous catalyst. It appears that catalysts based on aggregated nanoparticles suffer from coking to a larger extent in comparison to the nanofibrous samples.

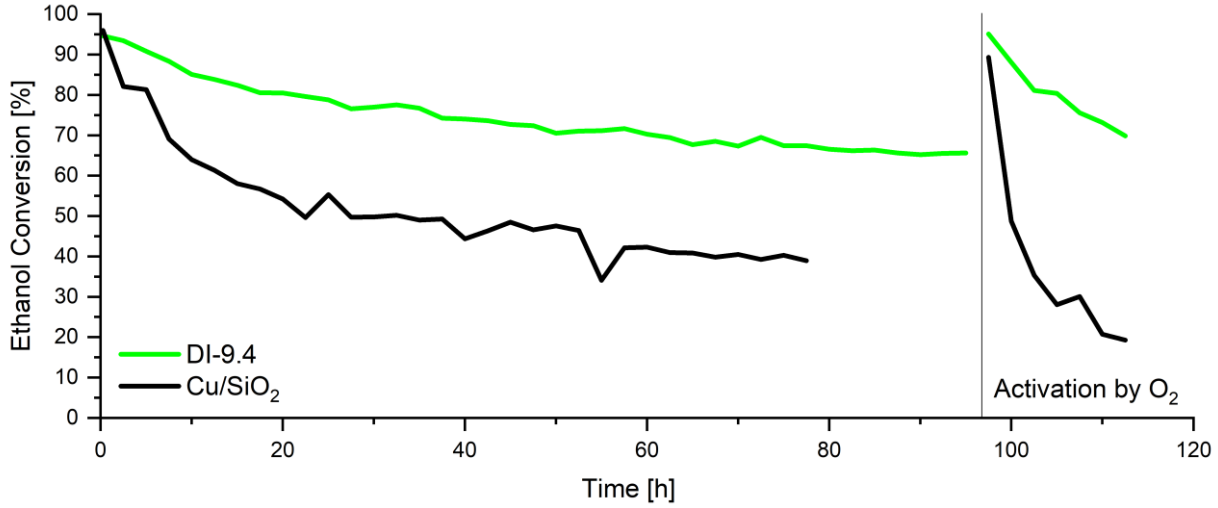

Figure 7. *Long-term stability test of DI-9.4 and comparison with a benchmark catalyst prepared by dry impregnation on conventional SiO_2 (Aerosil 300).*

3.4. Deactivation

The above-described catalytic stability and regeneration tests suggest that the main deactivation process is caused by coking. In good agreement with these results, the comparison of XRD diffractograms of fresh and spent catalysts shows no dramatic changes (**Figure 2**). While copper sintering on silica during catalysis is well documented in the literature,[14,18] the spent nanofibrous catalysts are still mostly XRD-amorphous. Spent catalyst **OP-6.5** showed a very weak and broad diffraction maximum at 45° (**Figure 2**, right). It reflects the starting formation of copper crystallites. Very small diffraction maxima were also observed for the **DI-9.4** sample. However, the application of the Debye-Scherrer equation was still not possible due to the low intensity of the diffraction maxima. The appearance of the first signs of diffractions could possibly indicate the beginning of some minor Cu particle and crystallite formation or sintering during the TOS.

The morphology of all spent catalysts was observed by the SEM method after the catalytic performance measurements (**Figure 8** and **Figure S7**)**.** In all cases, the nanofiber structure was partially damaged by handling, which resulted in the shortened length of the fibers. However, general morphology remained the same, featuring smooth fibers without apparent copper crystallization (proved by PXRD and STEM-EDS survey), again in good agreement with the stability of Cu against sintering on SiO_2 nanofibers. The STEM-EDS analyses performed on the spent Cu/SiO_2 NFs samples prepared by dry impregnation showed smooth fibrous morphology with homogeneous Cu distribution, similar to fresh **DI-5.1** and **DI-9.4** catalysts (**Figure 8** and **Figure S8**). Interestingly, the nanoparticles evidenced at the surface of the fresh **DI-1.8** (**Figure S4A**) were no longer observed (**Figure S8A**). In contrast to samples prepared by impregnation, the formation of relatively large particles was observed for the sample **OP-6.5** (**Figure S8D**). A more detailed STEM-EDS analysis confirmed that the particles consist of copper and that they are crystalline (**Figure S9**). The **OP-6.5** remains the only fibrous sample that exhibited extended copper mobility (in agreement with PXRD analyses).

N_2 porosimetry analyses were performed to observe the surface area changes upon catalytic testing. The results are listed in **Table S4**. The SSA analysis revealed that all samples lost a significant part of their surface area. The main part of porosity (up to 90 %) was represented by micropores and was blocked entirely apparently by coke production. All spent catalysts after TOS exhibited no micropores and a significant loss of surface area, particularly **DI-1.8** −99 %, **DI-9.4** −89 %, and **OP-6.5** −67 %, respectively. Despite the loss of microporosity, both **DI-9.4** and **OP-6.5** catalysts exhibited sustained high activity. This highlights the crucial role played by the external surface of nanofibers in catalysis.

The deactivation of prepared materials during catalysis was further investigated by TGA and XPS measurements (**Table 2**). Previous findings based on N_2 adsorption-desorption are in agreement with the TGA and XPS analyses, which found an excess of formed coke on the surface of the nanofiber catalysts (**Table 2**). Both methods are in good agreement for **OP-6.5** with the largest amount of carbon species deposited on the surface. A similar result of significantly higher coking was observed for a one-pot sample prepared by conventional hydrolytic sol-gel.[18] The Cu/SiO_2 NFs prepared by one-pot synthesis (**OP-6.5**) display a higher tendency toward coking than catalysts prepared by dry impregnation, resulting in less stable behavior of **OP-6.5** in comparison to **DI-5.1** at 325 °C. The surface carbon concentrations estimated by the XPS method after catalysis showed a similar amount of carbon in samples prepared by dry impregnation (5.22–5.45 wt%). Interestingly, the carbon content in **DI** catalysts was lower in comparison to **OP-6.5** (7.30 wt%), in agreement with TG analysis. An increased coke amount (**DI-1.8** > **DI-5.1** > **DI-9.4**) for **DI** samples observed by TGA correlates with the decreasing catalysts' stability at 325 °C.

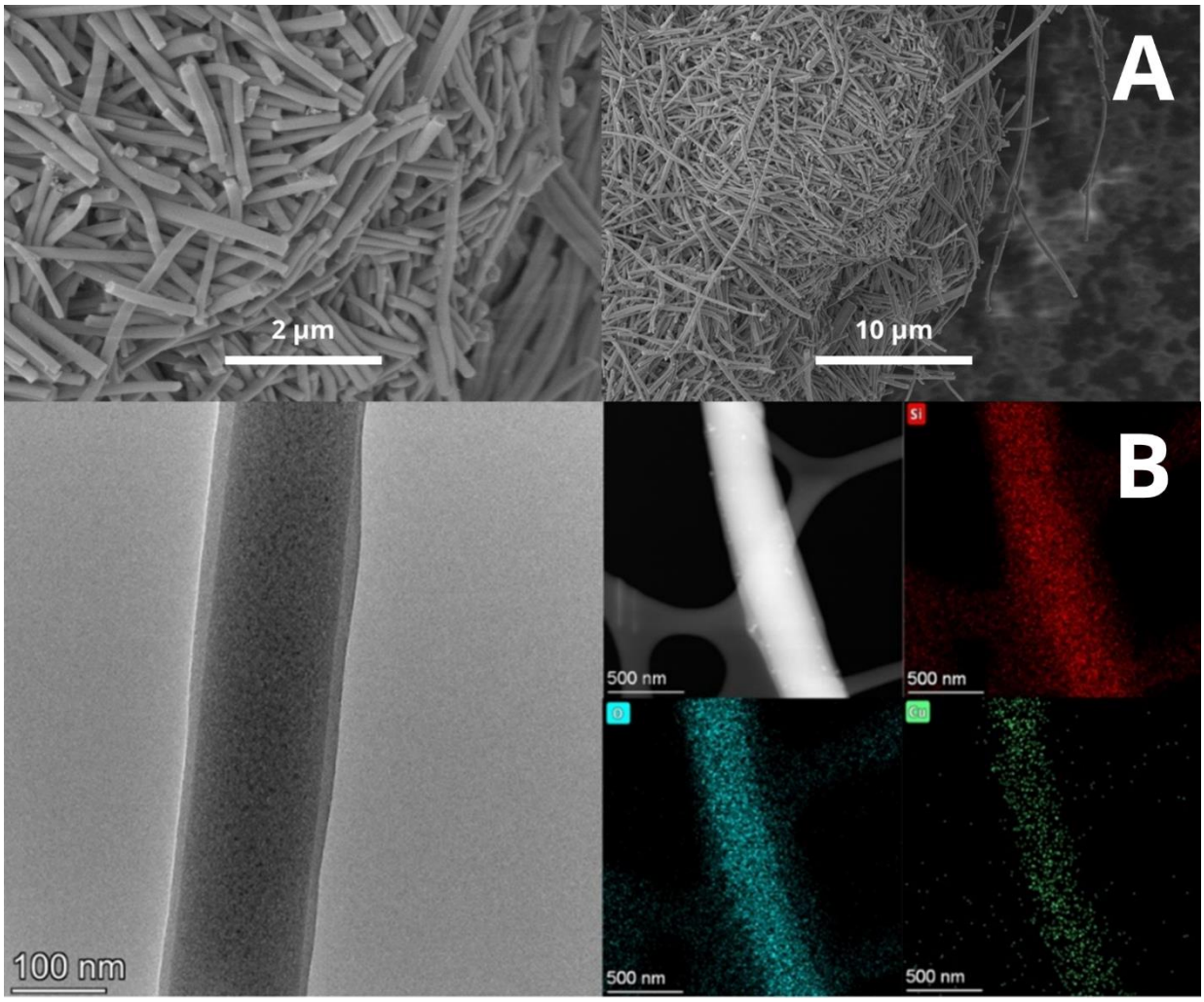

Figure 8. *A) SEM images of DI-9.4 sample after catalysis. B) STEM-EDS micrograph survey of spent DI-9.4 catalyst after 18 h of TOS. Red represents silicon, blue oxygen, and green copper in EDS analysis.)*

Table 2. *Study of catalyst coking by TGA and XPS methods.*

Preparation method	Mass change [%]		Coking by TGA [%]	Surface carbon content by XPS [wt%]		Carbon content increase [wt%]
	Fresh	Spent		Fresh	Spent	
DI-1.8	1.03	3.59	**2.56**	3.67	5.45	**+1.78**
DI-5.1	1.05	2.90	**1.85**	2.23	5.22	**+2.99**
DI-9.4	0.50	1.29	**0.79**	2.27	5.33	**+3.06**
OP-6.5	0.78	3.95	**3.17**	2.28	7.30	**+5.02**

4. Conclusions

In this study, we have successfully applied the electrospinning technique to synthesize remarkably thin SiO_2 nanofibers with 107 nm in diameter and surface area of 700 $m^2\ g^{-1}$. Nanofibers displayed a uniform and defect-free amorphous structure. Our method ensures a stable solution over time, facilitating reproducibility and scalability. These silica nanofibers were employed to prepare supported copper nanoparticles via dry impregnation, and their performance was compared to Cu/SiO_2 nanofibers prepared by a direct one-pot method based on electrospinning. The prepared nanofiber catalysts underwent testing in non-oxidative ethanol dehydrogenation to acetaldehyde within the temperature range of 185–290 °C and long-term test for 15 h at 325 °C. Our findings indicate that dry impregnation (**DI-5.1**) fibers outperformed the one-pot (**OP-6.5**) samples in catalytic tests. Importantly, a higher coking tendency was observed for one-pot synthesis. Moreover, increased copper loading of samples correlated with higher conversion rates and enhanced stability. Notably, **DI-9.4** at 325 °C achieved a 90 % ethanol conversion rate, remaining stable for 14 h with 93% selectivity to acetaldehyde (acetaldehyde productivity: 4.26 g g h^{-1}). A slow deactivation was observed during the long-term stability test and the nanofiber catalyst experienced a ~25% reduction of ethanol conversion after 100 h. Acetaldehyde productivity after 100 h of TOS reached 3.09 g g^{-1} h^{-1}; significantly higher than the catalyst with a similar Cu loading deposited on aggregated SiO_2 nanoparticles, highlighting the importance of support morphology in heterogeneous catalysis. The characterization of spent catalysts and the catalyst regeneration tests suggest that coking is the main reason for deactivation. The nanofibrous catalysts remain XRD-amorphous without significant Cu sintering after the catalytic tests.

Acknowledgments

We acknowledge Cryo-Electron Microscopy and Tomography Core Facility of CIISB, Instruct-CZ Centre, supported by MEYS CR (LM2018127). CzechNanoLab project LM2023051 funded by MEYS CR is gratefully acknowledged for the financial support of the measurements/sample fabrication at CEITEC Nano Research Infrastructure. This publication was supported by the project Quantum materials for applications in sustainable technologies (QM4ST), CZ.02.01.01/00/22_008/0004572 by Program J. A. Commenius, call Excellent Research.

References

(1) Grison, C.; Lock Toy Ki, Y. Ecocatalysis, a New Vision of Green and Sustainable Chemistry. *Curr. Opin. Green Sustain. Chem.* **2021**, *29*, 100461. DOI:10.1016/j.cogsc.2021.100461.

(2) Ren, T.; Patel, M.; Blok, K. Olefins from Conventional and Heavy Feedstocks: Energy Use in Steam Cracking and Alternative Processes. *Energy* **2006**, *31* (4), 425–451. DOI:10.1016/j.energy.2005.04.001.

(3) Ren, T.; Patel, M.; Blok, K. Steam Cracking and Methane to Olefins: Energy Use, CO_2 Emissions and Production Costs. *Energy* **2008**, *33* (5), 817–833. DOI:10.1016/j.energy.2008.01.002.

(4) Jira, R. Acetaldehyde from Ethylene—A Retrospective on the Discovery of the Wacker Process. *Angew. Chemie Int. Ed.* **2009**, *48* (48), 9034–9037. DOI:10.1002/anie.200903992.
(5) Seifzadeh Haghighi, S.; Rahimpour, M. R.; Raeissi, S.; Dehghani, O. Investigation of Ethylene Production in Naphtha Thermal Cracking Plant in Presence of Steam and Carbon Dioxide. *Chem. Eng. J.* **2013**, *228*, 1158–1167. DOI:10.1016/j.cej.2013.05.048.
(6) Fernandes, R. A.; Jha, A. K.; Kumar, P. Recent Advances in Wacker Oxidation: From Conventional to Modern Variants and Applications. *Catal. Sci. Technol.* **2020**, *10* (22), 7448–7470. DOI:10.1039/D0CY01820A.
(7) Gray, K. A.; Zhao, L.; Emptage, M. Bioethanol. *Curr. Opin. Chem. Biol.* **2006**, *10* (2), 141–146. DOI:10.1016/j.cbpa.2006.02.035.
(8) Sun, J.; Wang, Y. Recent Advances in Catalytic Conversion of Ethanol to Chemicals. *ACS Catal.* **2014**, *4* (4), 1078–1090. DOI:10.1021/cs4011343.
(9) Angelici, C.; Velthoen, M. E. Z.; Weckhuysen, B. M.; Bruijnincx, P. C. A. Influence of Acid–Base Properties on the Lebedev Ethanol-to-Butadiene Process Catalyzed by SiO_2 – MgO Materials. *Catal. Sci. Technol.* **2015**, *5* (5), 2869–2879. DOI:10.1039/C5CY00200A.
(10) Sushkevich, V. L.; Ivanova, I. I.; Ordomsky, V. V.; Taarning, E. Design of a Metal-Promoted Oxide Catalyst for the Selective Synthesis of Butadiene from Ethanol. *ChemSusChem* **2014**, *7* (9), 2527–2536. DOI:10.1002/cssc.201402346.
(11) Chagas, L. H.; Matheus, C. R. V.; Zonetti, P. C.; Appel, L. G. Butadiene from Ethanol Employing Doped T-ZrO_2. *Mol. Catal.* **2018**, *458*, 272–279. DOI:10.1016/j.mcat.2018.01.018.
(12) Goldemberg, J. Ethanol for a Sustainable Energy Future. *Science* **2007**, *315* (5813), 808–810. DOI:10.1126/science.1137013.
(13) Ob-eye, J.; Praserthdam, P.; Jongsomjit, B. Dehydrogenation of Ethanol to Acetaldehyde over Different Metals Supported on Carbon Catalysts. *Catalysts* **2019**, *9* (1), 66. DOI:10.3390/catal9010066.
(14) Pomalaza, G.; Arango Ponton, P.; Capron, M.; Dumeignil, F. Ethanol-to-Butadiene: The Reaction and Its Catalysts. *Catal. Sci. Technol.* **2020**, *10* (15), 4860–4911. DOI:10.1039/D0CY00784F.
(15) Zhang, H.; Tan, H. R.; Jaenicke, S.; Chuah, G. K. Highly Efficient and Robust Cu Catalyst for Non-Oxidative Dehydrogenation of Ethanol to Acetaldehyde and Hydrogen. *J. Catal.* **2020**, *389*, 19–28. DOI:10.1016/j.jcat.2020.05.018.
(16) Yu, D.; Dai, W.; Wu, G.; Guan, N.; Li, L. Stabilizing Copper Species Using Zeolite for Ethanol Catalytic Dehydrogenation to Acetaldehyde. *Chinese J. Catal.* **2019**, *40* (9), 1375–1384. DOI:10.1016/S1872-2067(19)63378-4.
(17) Pampararo, G.; Garbarino, G.; Riani, P.; Vykoukal, V.; Busca, G.; Debecker, D. P. Ethanol Dehydrogenation to Acetaldehyde with Mesoporous Cu-SiO2 Catalysts Prepared by Aerosol-Assisted Sol–Gel. *Chem. Eng. J.* **2023**, *465* (January), 142715. DOI:10.1016/j.cej.2023.142715.
(18) Pokorny, T.; Vykoukal, V.; Machac, P.; Moravec, Z.; Scotti, N.; Roupcova, P.; Karaskova, K.; Styskalik, A. Ethanol Dehydrogenation over Copper-Silica Catalysts: From Sub-Nanometer Clusters to 15 nm Large Particles. *ACS Sustain. Chem. Eng.* **2023**, *11* (30), 10980–10992. DOI:10.1021/acssuschemeng.2c06777.
(19) Sato, A. G.; Volanti, D. P.; De Freitas, I. C.; Longo, E.; Bueno, J. M. C. Site-Selective Ethanol Conversion over Supported Copper Catalysts. *Catal. Commun.* **2012**, *26*, 122–126. DOI:10.1016/j.catcom.2012.05.008.

(20) Freitas, I. C.; Damyanova, S.; Oliveira, D. C.; Marques, C. M. P.; Bueno, J. M. C. Effect of Cu Content on the Surface and Catalytic Properties of Cu/ZrO_2 Catalyst for Ethanol Dehydrogenation. *J. Mol. Catal. A Chem.* **2014**, *381*, 26–37. DOI:10.1016/j.molcata.2013.09.038.
(21) Fujita, S.; Iwasa, N.; Tani, H.; Nomura, W.; Arai, M.; Takezawa, N. Dehydrogenation of Ethanol Over Cu/ZnO Catalysts. *React. Kinet. Catal. Lett.* **2001**, *73* (2), 367–372. DOI:10.1023/A:1014192214324.
(22) Zhang, H.; Tan, H.-R.; Jaenicke, S.; Chuah, G.-K. Highly Efficient and Robust Cu Catalyst for Non-Oxidative Dehydrogenation of Ethanol to Acetaldehyde and Hydrogen. *J. Catal.* **2020**, *389*, 19–28. DOI:10.1016/j.jcat.2020.05.018.
(23) Chang, F.-W.; Yang, H.-C.; Roselin, L. S.; Kuo, W.-Y. Ethanol Dehydrogenation over Copper Catalysts on Rice Husk Ash Prepared by Ion Exchange. *Appl. Catal. A Gen.* **2006**, *304* (1–2), 30–39. DOI:10.1016/j.apcata.2006.02.017.
(24) Yu, J.; Yang, M.; Zhang, J.; Ge, Q.; Zimina, A.; Pruessmann, T.; Zheng, L.; Grunwaldt, J.-D.; Sun, J. Stabilizing Cu^+ in Cu/SiO_2 Catalysts with a Shattuckite-Like Structure Boosts CO 2 Hydrogenation into Methanol. *ACS Catal.* **2020**, *10* (24), 14694–14706. DOI:10.1021/acscatal.0c04371.
(25) Huo, D.; Kim, M. J.; Lyu, Z.; Shi, Y.; Wiley, B. J.; Xia, Y. One-Dimensional Metal Nanostructures: From Colloidal Syntheses to Applications. *Chem. Rev.* **2019**, *119* (15), 8972–9073. DOI:10.1021/acs.chemrev.8b00745.
(26) Dankeaw, A.; Gualandris, F.; Silva, R. H.; Scipioni, R.; Hansen, K. K.; Ksapabutr, B.; Esposito, V.; Marani, D. Highly Porous Ce–W–TiO_2 Free-Standing Electrospun Catalytic Membranes for Efficient de-NOx via Ammonia Selective Catalytic Reduction. *Environ. Sci. Nano* **2019**, *6* (1), 94–104. DOI:10.1039/C8EN01046C.
(27) Loccufier, E.; Debecker, D. P.; D'hooge, D. R.; De Buysser, K.; De Clerck, K. Fibrous Material Structure Developments for Sustainable Heterogeneous Catalysis – An Overview. *ChemCatChem* **2024**, *202301563*, 1–13. DOI:10.1002/cctc.202301563.
(28) Xue, J.; Wu, T.; Dai, Y.; Xia, Y. Electrospinning and Electrospun Nanofibers: Methods, Materials, and Applications. *Chem. Rev.* **2019**, *119* (8), 5298–5415. DOI:10.1021/acs.chemrev.8b00593.
(29) Drew, C.; Wang, X.; Samuelson, L. A.; Kumar, J. The Effect of Viscosity and Filler on Electrospun Fiber Morphology. *J. Macromol. Sci. Part A* **2003**, *40* (12), 1415–1422. DOI:10.1081/MA-120025320.
(30) Forward, K. M.; Rutledge, G. C. Free Surface Electrospinning from a Wire Electrode. *Chem. Eng. J.* **2012**, *183*, 492–503. DOI:10.1016/j.cej.2011.12.045.
(31) Ramaseshan, R.; Sundarrajan, S.; Jose, R.; Ramakrishna, S. Nanostructured Ceramics by Electrospinning. *J. Appl. Phys.* **2007**, *102* (11). DOI:10.1063/1.2815499.
(32) Kundrat, V.; Vykoukal, V.; Moravec, Z.; Simonikova, L.; Novotny, K.; Pinkas, J. Preparation of Polycrystalline Tungsten Nanofibers by Needleless Electrospinning. *J. Alloys Compd.* **2022**, *900*, 163542. DOI:10.1016/j.jallcom.2021.163542.
(33) Dong, S.; Maciejewska, B. M.; Schofield, R. M.; Hawkins, N.; Siviour, C. R.; Grobert, N. Electrospinning Nonspinnable Sols to Ceramic Fibers and Springs. *ACS Nano* **2024**, *nn-2023-12*. DOI:10.1021/acsnano.3c12659.
(34) Kundrat, V.; Patak, A.; Pinkas, J. Preparation of Ultrafine Fibrous Uranium Dioxide by Electrospinning. *J. Nucl. Mater.* **2020**, *528*, 151877. DOI:10.1016/j.jnucmat.2019.151877.
(35) Kundrat, V.; Moravec, Z.; Pinkas, J. Preparation of Thorium Dioxide Nanofibers by

Electrospinning. *J. Nucl. Mater.* **2020**, *534*, 152153. DOI:10.1016/j.jnucmat.2020.152153.
(36) Patel, A. C.; Li, S.; Wang, C.; Zhang, W.; Wei, Y. Electrospinning of Porous Silica Nanofibers Containing Silver Nanoparticles for Catalytic Applications. *Chem. Mater.* **2007**, *19* (6), 1231–1238. DOI:10.1021/cm061331z.
(37) Ding, B.; Kim, H.; Kim, C.; Khil, M.; Park, S. Morphology and Crystalline Phase Study of Electrospun TiO_2 SiO_2 Nanofibres. *Nanotechnology* **2003**, *14* (5), 532–537. DOI:10.1088/0957-4484/14/5/309.
(38) Di Mauro, A.; Fragalà, M. E. Electrospun SiO_2 "Necklaces" on Unglazed Ceramic Tiles: A Planarizing Strategy. *Superlattices Microstruct.* **2015**, *81*, 265–271. DOI:10.1016/j.spmi.2015.01.027.
(39) Teng, M.; Qiao, J.; Li, F.; Bera, P. K. Electrospun Mesoporous Carbon Nanofibers Produced from Phenolic Resin and Their Use in the Adsorption of Large Dye Molecules. *Carbon N. Y.* **2012**, *50* (8), 2877–2886. DOI:10.1016/j.carbon.2012.02.056.
(40) Talebian, S.; Afifi, A. M.; Hatami, M.; Bazgir, S.; Khanlou, H. M. Preparation and Characterisation of Electrospun Silica Nanofibres. *Mater. Res. Innov.* **2014**, *18* (sup6), S6-510-S6-514. DOI:10.1179/1432891714Z.0000000001034.
(41) Shao, C.; Kim, H.; Gong, J.; Lee, D. A Novel Method for Making Silica Nanofibres by Using Electrospun Fibres of Polyvinylalcohol/Silica Composite as Precursor. *Nanotechnology* **2002**, *13* (5), 635–637. DOI:10.1088/0957-4484/13/5/319.
(42) Choi, S.; Lee, S. G.; Im, S. S.; Kim, S. H.; Joo, Y. L. Silica Nanofibers from Electrospinning/Sol-Gel Process. *J. Mater. Sci. Lett.* **2003**, *22* (12), 891–893. DOI:10.1023/a:1024475022937.
(43) Zhao, Y.; Wang, H.; Lu, X.; Li, X.; Yang, Y.; Wang, C. Fabrication of Refining Mesoporous Silica Nanofibers via Electrospinning. *Mater. Lett.* **2008**, *62* (1), 143–146. DOI:10.1016/j.matlet.2007.04.096.
(44) Geltmeyer, J.; Van Der Schueren, L.; Goethals, F.; De Buysser, K.; De Clerck, K. Optimum Sol Viscosity for Stable Electrospinning of Silica Nanofibres. *J. Sol-Gel Sci. Technol.* **2013**, *67* (1), 188–195. DOI:10.1007/s10971-013-3066-x.
(45) Kanehata, M.; Ding, B.; Shiratori, S. Nanoporous Ultra-High Specific Surface Inorganic Fibres. *Nanotechnology* **2007**, *18* (31), 315602. DOI:10.1088/0957-4484/18/31/315602.
(46) Chen, Y.; Zhang, Z.; Yu, J.; Guo, Z. Poly(Methyl Methacrylate)/Silica Nanocomposite Fibers by Electrospinning. *J. Polym. Sci. Part B Polym. Phys.* **2009**, *47* (12), 1211–1218. DOI:10.1002/polb.21727.
(47) Liu, Y.; Huang, H.; Wang, L.; Cai, D.; Liu, B.; Wang, D.; Li, Q.; Wang, T. Electrospun CeO2 Nanoparticles/PVP Nanofibers Based High-Frequency Surface Acoustic Wave Humidity Sensor. *Sensors Actuators, B Chem.* **2016**, *223*, 730–737. DOI:10.1016/j.snb.2015.09.148.
(48) Schneider, C. A.; Rasband, W. S.; Eliceiri, K. W. NIH Image to ImageJ: 25 Years of Image Analysis. *Nat. Methods* **2012**, *9* (7), 671–675. DOI:10.1038/nmeth.2089.
(49) Biesinger, M. C.; Hart, B. R.; Polack, R.; Kobe, B. A.; Smart, R. S. C. Analysis of Mineral Surface Chemistry in Flotation Separation Using Imaging XPS. *Miner. Eng.* **2007**, *20* (2), 152–162. DOI:10.1016/j.mineng.2006.08.006.
(50) Pampararo, G.; Garbarino, G.; Riani, P.; Villa García, M.; Sánchez Escribano, V.; Busca, G. A Study of Ethanol Dehydrogenation to Acetaldehyde over Supported Copper Catalysts: Catalytic Activity, Deactivation and Regeneration. *Appl. Catal. A Gen.* **2020**, *602* (June), 117710. DOI:10.1016/j.apcata.2020.117710.

(51) Pokorny, T.; Doroshenko, I.; Machac, P.; Simonikova, L.; Bittova, M.; Moravec, Z.; Karaskova, K.; Skoda, D.; Pinkas, J.; Styskalik, A. Copper Phosphinate Complexes as Molecular Precursors for Ethanol Dehydrogenation Catalysts. *Inorg. Chem.* **2023**. DOI:10.1021/acs.inorgchem.3c01678.
(52) Barr, T. L.; Seal, S. Nature of the Use of Adventitious Carbon as a Binding Energy Standard. *J. Vac. Sci. Technol. A Vacuum, Surfaces, Film.* **1995**, *13* (3), 1239–1246. DOI:10.1116/1.579868.
(53) Mitchell, D. F.; Clark, K. B.; Bardwell, J. A.; Lennard, W. N.; Massoumi, G. R.; Mitchell, I. V. Film Thickness Measurements of SiO_2 by XPS. *Surf. Interface Anal.* **1994**, *21* (1), 44–50. DOI:10.1002/sia.740210107.
(54) Styskalik, A.; Kordoghli, I.; Poleunis, C.; Delcorte, A.; Aprile, C.; Fusaro, L.; Debecker, D. P. Highly Porous Hybrid Metallosilicate Materials Prepared by Non-Hydrolytic Sol-Gel: Hydrothermal Stability and Catalytic Properties in Ethanol Dehydration. *Microporous Mesoporous Mater.* **2020**, *297*, 110028. DOI:10.1016/j.micromeso.2020.110028.
(55) Post, P.; Wurlitzer, L.; Maus-Friedrichs, W.; Weber, A. Characterization and Applications of Nanoparticles Modified In-Flight with Silica or Silica-Organic Coatings. *Nanomaterials* **2018**, *8* (7), 530. DOI:10.3390/nano8070530.
(56) Petrolini, D. D.; Cassinelli, W. H.; Pereira, C. A.; Urquieta-González, E. A.; Santilli, C. V.; Martins, L. Ethanol Dehydrogenative Reactions Catalyzed by Copper Supported on Porous Al–Mg Mixed Oxides. *RSC Adv.* **2019**, *9* (6), 3294–3302. DOI:10.1039/C8RA10076D.